A R C H I V E S O F M E T A L L U R G Y A N D M A T E R I A L S
Volume 56 2011 Issue 4
DOI: 10.2478/v10172-011-0127-4

H. BERNARD*, A. LISIŃSKA-CZEKAJ*, J. DZIK*, K. OSIŃSKA*, D. CZEKAJ*

FABRICATION, STRUCTURAL AND AC IMPEDANCE STUDIES OF LAYER–STRUCTURED $Bi_4Ti_3O_{12}$ CERAMICS

WYTWARZANIE, STRUKTURA ORAZ BADANIA IMPEDANCYJNE WARSTWOWEJ CERAMIKI $Bi_4Ti_3O_{12}$

In the present research bismuth titanate $Bi_4Ti_3O_{12}$ (BiT) ceramics was synthesized by the standard solid-state reaction method from the mixture of oxides, followed by free sintering at temperature T=1000°C. BiT ceramics was studied in terms of its chemical composition (EDS), crystalline structure (X-ray), microstructure (SEM) and dielectric properties (ac technique of complex impedance spectroscopy) over a range of frequency (f=100Hz to f=1MHz) and temperature (T=200-500°C). Experimental results confirmed the phase formation. It was found that BiT ceramics crystallized in orthorhombic symmetry, best described with *Fmmm* space group and the following elementary cell parameters: a=5.409(6)Å, b=5.449(2)Å and c=32.816(2)Å. It was also found that BiT ceramics exhibited the plate–like microstructure and stoichiometric chemical composition. Impedance spectroscopy measurements showed contribution of three overlapping relaxation processes (three semicircles in the complex impedance diagrams were observed) ascribed to bulk, grain boundary and electrode/interface polarization phenomena. Impedance data were fitted to the corresponding equivalent circuit using the complex nonlinear least squares (CNLS) method. The ac conductivity for grains, grain boundaries and electrode processes was calculated from CNLS fit of the impedance data and thus the activation energy of ac conductivity (σ_{AC}) and relaxation (τ) was calculated for the three revealed components of the impedance spectra from the slopes of σ_{AC} and τ versus 1000/T plots (semi log scale) in the range of ΔT=200–500°C.

Keywords: bismuth titanate, Aurivillius phase, impedance spectroscopy

W prezentowanej pracy ceramikę tytanianu bizmutu $Bi_4Ti_3O_{12}$ (BiT) syntezowano metodą reakcji w fazie stałej z mieszaniny prostych tlenków w T=1000°C. Zbadano skład chemiczny (EDS), strukturę krystaliczną (X-ray), mikrostrukturę (SEM) oraz właściwości dielektryczne metodą spektroskopii impedancyjnej w zakresie częstotliwości od f=100Hz do f=1MHz w temperaturze T=200-500°C. Analizując obraz SEM można zauważyć, że płytkopodobne ziarna tworzą liczne, rozgałęzione pręty. Wyniki eksperymentalne potwierdziły wytworzenie się fazy krystalicznej BiT. Ceramika BiT krystalizuje w symetrii rombowej, opisywana jest grupą przestrzenną *Fmmm*, charakteryzuje się parametrami komórki: a=5.409(6)Å, b=5.449(2)Å, c=32.816(2)Å.

Pomiary spektroskopii impendancyjnej wykazały udział trzech nakładających się procesów relaksacyjnych (zaobserwowano trzy półkola przedstawione w diagramach impedancji) przypisanych wnętrzu ziaren, granicy ziaren oraz zjawisk polaryzacji na granicy powierzchni elektroda/próbka.

Dane impedancyjne przybliżono odpowiednimi schematami zastępczymi przy użyciu metody złożonych, nieliniowych, najmniejszych kwadratów (CNLS). Wyznaczono przewodnictwo zmiennoprądowe dla ziaren, granic ziaren i procesów elektrodowych oraz energię aktywacji przewodnictwa E_a^c i relaksacji E_a^t w zakresie temperatur ΔT=200–500°C.

1. Introduction

The family of oxides having bismuth oxide layers alternating with perovskite structure layers, known as perovskite layered structures, were discovered by Aurivillius [1-3]. Since the discovery, more than fifty compounds have been found to adopt this type of structure and many have shown to exhibit displacive ferroelectric transitions. The crystal structure of bismuth layer-structured ferroelectrics (BLSFs) may be described as a stacking of bismuth oxide layers $(Bi_2O_2)^{2+}$ and perovskite layers $(A_{m-1}B_mO_{3m-1})^{2-}$ along the pseudotetragonal c axis. Here A can be mono-, di- or trivalent ions or a mixture of them, where B represents Ti^{4+}, Nb^{5+}, Mo^{6+}, W^{6+}, Fe^{3+}. In the $(A_{m-1}B_mO_{3m-1})^{2-}$ units, B ions are enclosed by oxygen octahedral, which are linked through corners forming O-B-O linear chains. A ions occupy the spaces in the framework of BO_6octahedral. The perovskite slab

* UNIVERSITY OF SILESIA, DEPARTMENT OF MATERIALS SCIENCE, 41-200 SOSNOWIEC, 2 ŚNIEŻNA STR., POLAND

contains (m) oxygen regular octahedrons along its thickness. Adjacent perovskite-like layers are displaced in relation to each other for $a_0/\sqrt{2}$ in [110] direction, where a_0 is the prototype lattice parameter (regular perovskite cell) [4-6].

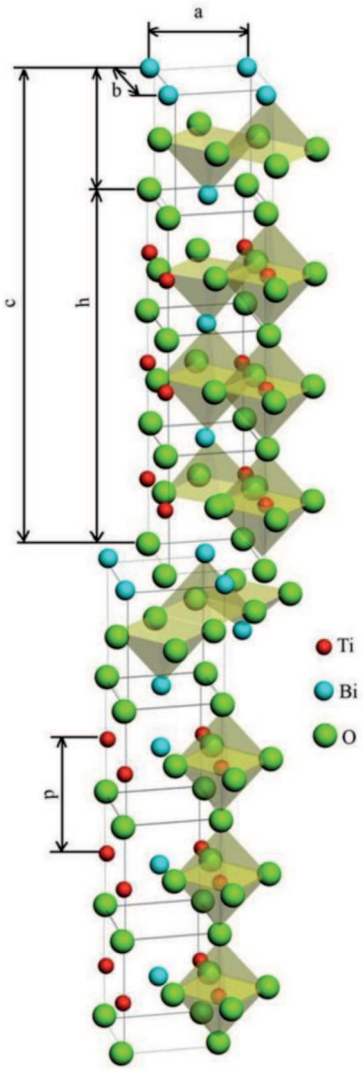

Fig. 1. Structure of $A_{m-1}Bi_2M_mO_{3m+3}$ Aurivillius phase for m=3 [16]

Archetypal members of the Aurivillius family are therefore Bi_2WO_6 (m=1), $SrBi_2Ta_2O_9$ (m=2) and $Bi_4Ti_3O_{12}$ (m=3). As shown in Fig. 1 for the case of $Bi_4Ti_3O_{12}$ (BiT) the structure can be envisaged as layers of corner-connected octahedrally coordinated ions, separated by $(Bi_2O_2)^{2+}$ layers [4]. The layers with the octahedrally coordinated ions i.e., $(Bi_2Ti_3O_{10})^{2-}$ layers, look like slabs of the perovskite structure. That is to say that Ti ions are enclosed by oxygen octahedral, which are linked through corners forming O-Ti-O linear chains. Bi ions occupy the spaces in the framework of TiO_6 octahedral. The height of the perovskite-type layer sandwiched between Bi_2O_2 layers in $Bi_4Ti_3O_{12}$ is equal to six O-Ti-O distances or approximately to m=3 ABO_3 perovskite units [7].

It has been shown [7, 8] that when the perovskite block is an even number of octahedral thick, the symmetry imposes a restriction on the polarization direction, confining it to the $a-b$ plane. In contrast, when the perovskite block is an odd number of octahedral thick, it is possible to develop a component of the polarization along the c-axis (nearly perpendicular to the layers). It has important implications for the use of the bismuth layer perovskites structure. Since there are comparatively few allowed directions for the spontaneous polarization, the remanent polarization is rather small for many film orientations.

Bismuth titanate, $Bi_4Ti_3O_{12}$ (BiT; m=3) is one of the best studied member of the BLSFs, and wide variety of solid solutions based on BiT have successfully been synthesized [e.g. 9, 10]. It is a well-known candidate for high temperature piezoelectric applications, memory storage, and optical display devices due to its high Curie temperature (T~675°C), a good resistance vs temperature, low dielectric dissipation, a relatively high dielectric constant $\varepsilon\approx200$ and an anisotropic nature originating from its layered structure [11, 12]. Excellent electrical and even electro-optic properties could be achieved in ferroelectric films of BiT [13].

Electrical and physical properties of bismuth titanate layer-structured ferroelectrics can be formed and /or changed due to their large possibilities of changing (their) chemical composition (e.g. by ionic substitutions in A and B positions) and crystalline structure (due to displacement of ions from their regular positions, twist of octahedral chains or displacement of ions with mutual twist of octahedrons).

In the present study the authors have focused on fabrication of $Bi_4Ti_3O_{12}$ ceramics by mixed oxide method followed by free sintering and characterizing it from the point of view of its thermal behavior, crystalline structure, microstructure, chemical composition and ac impedance behavior at low frequency (f=100Hz–1MHz) and in the temperature range up to T=500°C.

2. Experimental

The synthesis of $Bi_4Ti_3O_{12}$ ceramic powders was performed according to the formula:

$$2Bi_2O_3 + 3TiO_2 \rightarrow Bi_4Ti_3O_{12} \qquad (1)$$

from the stoichiometric mixture of bismuth oxide Bi_2O_3 (99.9% ALDRICH) and titanium oxide TiO_2 (99.9% POCH) by the standard mixed oxide method (MOM).

The consolidation of the powders was reached by free sintering method at T=1000°C. The soaking time of the sintering process was t=2h.

Simultaneous thermal analysis (STA), was used to investigate synthesis effects in the stoichiometric mixture of powders in which both thermal analysis (DTA) and mass change effects (TG) are measured concurrently on the same sample. The measurements were obtained with Netzsch STA409 thermal analyzer which is a combined DTA/TG/DTG system. The heating rate was κ=10°C/min.

Microstructure of the ceramic samples was observed by scanning electron microscopy with HITACHI S-4700–type equipment. The stoichiometry of $Bi_4Ti_3O_{12}$ ceramics was studied with the EDS chemical composition analysis system. The X-ray patterns were recorded in a 2Θ range from 10° to 105° with the X'Pert Pro diffractometer in the Θ-2Θ mode at room temperature using CoKα radiation, detector scan step $\Delta 2\Theta$=0.01° and a counting time t=7s. The analysis of the X-ray diffraction patterns of the ceramic powders was carried out using the X'Pert HighScore Plus software (PANalytical B.V). X'Pert HighScore Plus program has enabled phase analysis, using the latest available ICSD and ICDD database. The phase analysis was also conducted using freeware databases IUCr/COD/AMCSD using the Match! -computer program (Crystal Impact, Inc.). Microstructure and crystalline structure studies were carried out at room temperature.

For impedance measurements, sintered samples were polished and silver paste was deposited on both sides. The ac impedance behavior of $Bi_4Ti_3O_{12}$ ceramics were studied with the impedance analyzer of HP4192A type. All impedance data were fitted to appropriate equivalent circuits using ZView Software (Scribner Associates, Inc.). The validity of the CNLS (complex non-linear least squares method [14]) fitting procedure was estimated according to the following methods: χ-squared and the weighted sum of squares, referred to as χ^2 and WSS [15]. In the present study we chose a "modulus data weighting" [16].

3. Results and discussion

The results of the simultaneous thermal analysis of the stoichiometric mixture of starting oxides, i.e. Bi_2O_3 and TiO_2 that were used for synthesis of $Bi_4Ti_3O_{12}$ ceramics are given in Fig.2. One can see from Fig. 2 that the mass loss starts at about T=250°C and finishes at about T=500°C. The total value of the mass loss measured at T=500°C is rather small and amounts to Δm=0.29%. No DTA peak corresponds to this mass change effect.

Taking into account the results of thermal analysis of pure titanium oxide and bismuth oxide [4] one can say that pure TiO_2 titanium oxide does not exhibit any thermal events being heated to temperature T=1300°C while pure Bi_2O_3 suffers phase transitions (exemplified as peaks on DTA curve) from the monoclinic δ-phase to the high temperature cubic phase at approximately T=730°C. The δ-phase is stable up to its melting point at approximately T=825°C [4]. No such effects are visible on thermal analysis curves of the stoichiometric mixture of oxides given in Fig. 2.

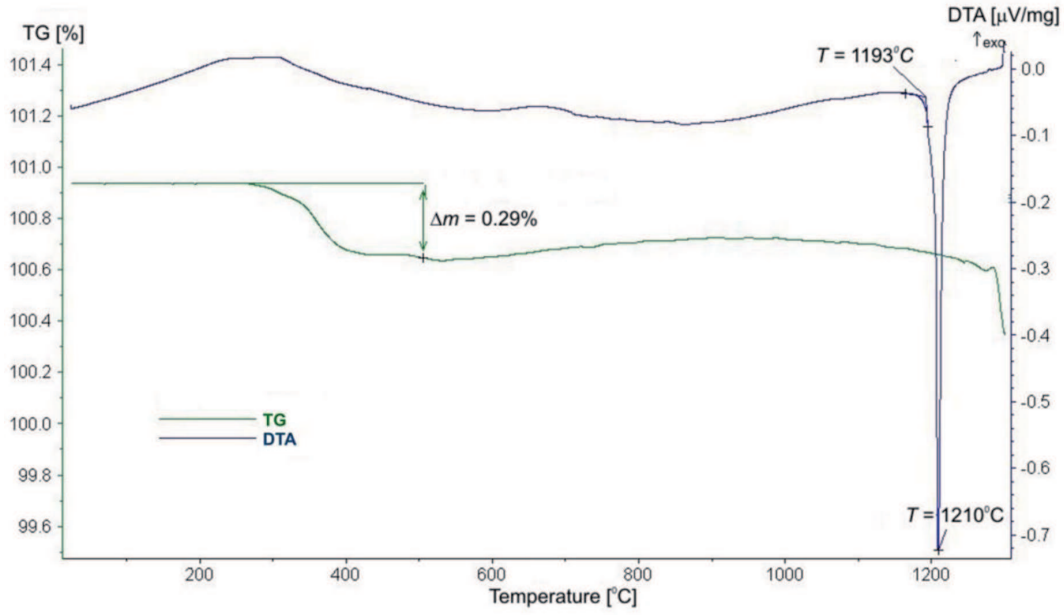

Fig. 2. Thermal analysis data of stoichiometric mixture of powders, viz. $2Bi_2O_3$ + $3TiO_2$ leading to formation of $Bi_4Ti_3O_{12}$ compound

According to the experimental data on mechanism of formation of $Bi_4Ti_3O_{12}$ [17] its thermal behavior and crystal structure [18], $Bi_4Ti_3O_{12}$ formation occurs by the mechanism of successive rearrangements of α-Bi_2O_3 into $Bi_{12}TiO_{20}$ (initiated by incorporation of titanium dioxide into Bi_2O_3 structure) and $Bi_{12}TiO_{20}$ into $Bi_4Ti_3O_{12}$ (transport processes) [17]. Formation of an intermediate $Bi_{12}TiO_{20}$ phase, determined from X-ray analysis and reported in [17], starts at about T=300°C reaches its maximum value at about T=550°C. With a further increase in temperature up to T=800°C the amount of $Bi_{12}TiO_{20}$ phase monotonously decays to zero. Within the temperature range ΔT=500–800°C formation of $Bi_4Ti_3O_{12}$ phase takes place [17]. Taking into account the above results the mass loss observed in Fig. 2 can be assigned to the formation of an intermediate $Bi_{12}TiO_{20}$ phase whereas formation of $Bi_4Ti_3O_{12}$ occurs without a mass loss.

The sharp endothermic peak on DTA curve at T=1210°C (onset at T=1193°C; Fig. 2) is in a good agreement with both differential thermal analysis and differential scanning calorimetry data performed for synthesized $Bi_4Ti_3O_{12}$ compound. One can state that the peak corresponds to the solidus temperature of the synthesized materials [18, 19].

Fig. 3. shows the SEM images and EDS spectrum of BiT ceramic samples fabricated by free sintering at T=1000°C. One can see from Fig. 3 that microstructure of BiT ceramics consists of unusually straight and orthogonally branched rods and well packed platelets. The grains exhibited a plate-like shape and were about d=0.1μm wide and l=0.2μm long. It is usually thought [1] that the plate-like grains are useful as materials for making grain-oriented ferroelectric ceramics. Stoichiometric ratio of the main metallic components was calculated for simple oxides Bi_2O_3 and TiO_2 on the base of EDS measurements and the results of such calculation are presented in Tab.1 where both theoretical and experimental content of elements for $Bi_4Ti_3O_{12}$ ceramics can be compared. It can be seen from Tab. 1 that BiT ceramics fabricated according to our technology exhibited stoichiometric composition with an accuracy typical for the measuring method applied.

TABLE 1
Theoretical and experimental content of elements (calculation for simple oxides) for $Bi_4Ti_3O_{12}$ ceramic

Formula	Theoretic contents of oxides [%]	Content of oxides from EDS [%]
Bi_2O_3	79.55	79.58
TiO_2	20.45	20.42

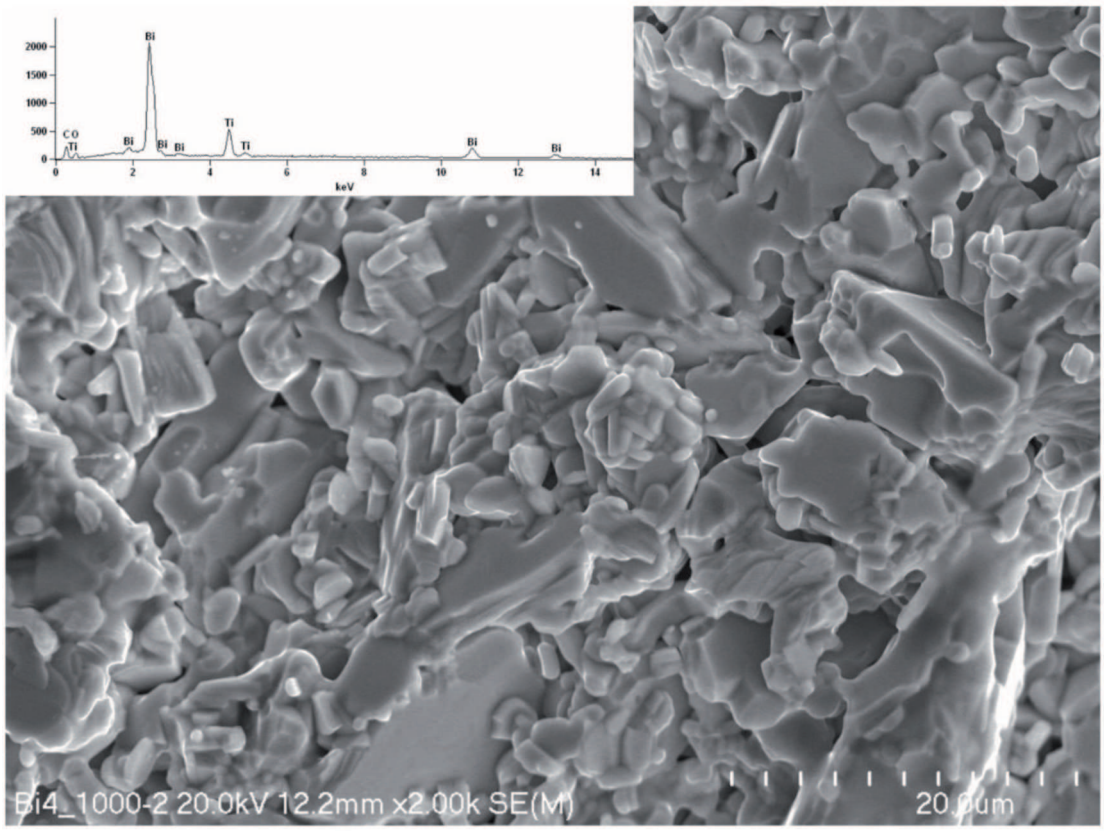

Fig. 3. SEM micrograph and analysis spectrum EDS of $Bi_4Ti_3O_{12}$ ceramic prepared by free sintering at T=1000°C

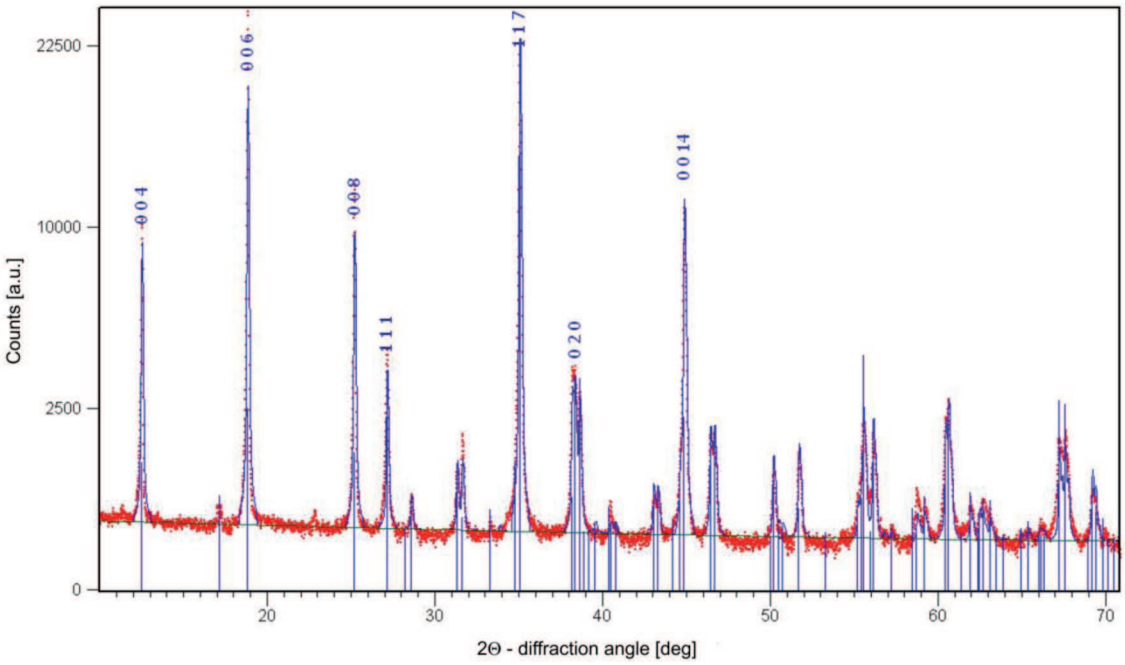

Fig. 4. X-ray diffraction pattern of $Bi_4Ti_3O_{12}$ ceramic powder at room temperature

The room temperature X-ray diffraction pattern of $Bi_4Ti_3O_{12}$ ceramic powder is shown in Fig.4. The structure of $Bi_4Ti_3O_{12}$ was found as orthorhombic (space group *Fmmm*) with the following unit cell parameters: a=5.409(6)Å, b=5.449(2)Å and c=32.816(2)Å. A more detailed description of the X-ray analysis performed for the fabricated ceramics can be found elsewhere [20].

Impedance spectroscopy (IS) was utilized for characterization of BiT ceramics. It is a powerful method of characterizing many of the electrical properties of materials and their interfaces with electronically conducting electrodes. A great strength of impedance spectroscopy lies in the fact that, with the appropriate data analysis, it is often possible to characterize the different electrically active regions in a material by demonstrating their existence and by measuring their individual electric properties [21, 22].

In the present study the complex impedance formalism expressed as:

$$Z^* = Z' - jZ'' = R_S - \frac{j}{\omega C_S} \qquad (2)$$

was used. Z' and Z'' are the real and imaginary components of impedance, ω=2πf– angular frequency, R_S and C_S are series components of equivalent circuit components, i.e. resistance and capacitance, respectively.

The idealized plot in the complex plane (i.e. Z'' vs. Z') that describes a polycrystalline oxide material usually includes three components with their corresponding relaxation frequencies. At higher frequencies the component normally corresponds to the bulk properties, at intermediate frequency the element corresponds to the grain boundaries and at low frequency the contribution of electrode processes or processes occurring at electrode/interface are represented [21, 22].

Visual analysis of the individual IS data plots given in Fig. 5 (T=200°C (a), T=400°C (b), T=500°C (c)) have shown that the experimental points form smooth curves with three partially overlapping depressed semicircles (Fig. 5, open circles). To check the quality of the impedance data, which is essential for a proper CNLS analysis [14], the Kramers–Kronig (K-K) validation tests were performed.

In this connection it is worth noting that the CNLS method centers on minimizing the object function S with respect to the parameters a_k of the model function $Z^*(\nu, a_k)$:

$$S = \sum_{i=1}^{N} w_i \left\{ \left[Z_i' - Z'(\nu_i, a_k) \right] r + \left[Z_i'' - Z''(\nu_i, a_k) \right]^2 \right\}, \quad (3)$$

where $Z_i' - jZ_i''$ represent the measured impedance at frequency ν_i and w_i is the weight factor. However, it is sometimes difficult to obtain an acceptable match between measurement and model. The reason can be an inadequate model function or date that is corrupted by a systematic deviation. Therefore it is important to discern between "bad" data and an inappropriate model function.

The Kramers-Kroning relation present a very useful tool for data validation [23]. The Kramers-Kroning rule states that the imaginary part of the dispersion is completely determined by the form of the real part and

vice-versa – the real part is determined by imaginary dispersion over the frequency range $0 \leqslant \nu \leqslant \infty$. These relations can be expressed for real and imaginary part of impedance or admittance and found in literature [eg. 6, 23]. In the course of the present study the computer program by B.A.Boulamp was used [23, 24] for performing the K-K validation tests.

a)

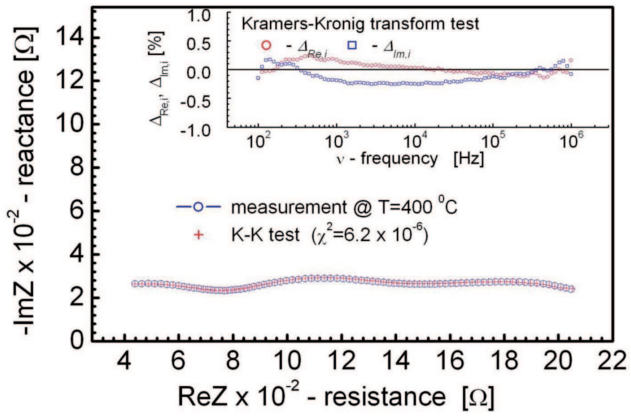

b)

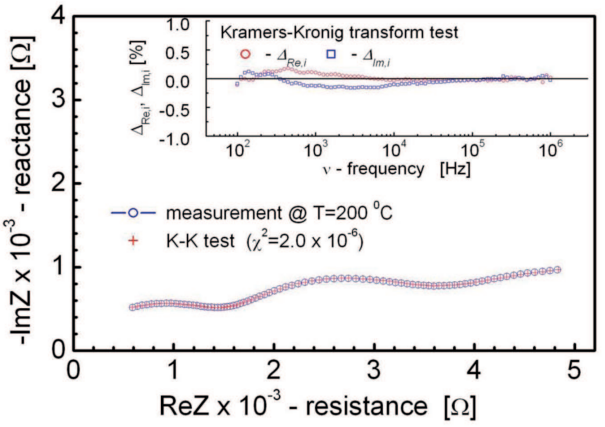

c)

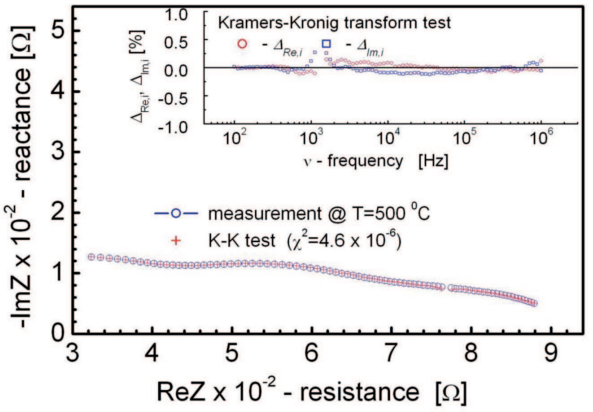

Fig. 5. Impedance diagram for $Bi_4Ti_3O_{12}$ ceramics at T=200°C (a), T=400°C (b), T=500°C (c), open circles, measured data, crosses, Kramers-Kronig transform test results. The insets show results of the K-K test in the form of the relative differences plot

The results of the K-K validation test are shown as insets in Fig. 5a,b,c. The resulting "pseudo Chi-squared" value is also shown in the figure.

An important control tool is the distribution of the residuals versus frequency. It is commonly known [eg. 14, 21-24] that for a correct impedance data set, the relative differences between the measured and calculated value for the real part of impedance and the imaginary part (residuals) should be randomly distributed around the log(ν) axis.

In the present case, as indicated in the insets of Fig. 5, one can see a clear trace which shows deviation from K-K behavior. The deviation, however, is quite small as the residuals are less than 0.5%. The combination of the measured data (open circles) and its K-K transformation (crosses) shown in Fig. 5 proves that the impedance data of $Bi_4Ti_3O_{12}$ ceramics is of a good quality and can be used for the further analysis.

In order to extract as much information as possible from impedance measurements, the experimental spectra were subjected to CNLS fitting procedure with ZView computer program (Scribner Associates, Inc.). The elements of an equivalent circuit model represent the various (macroscopic) processes involved in the transport of mass and charge. Equivalent circuit used for impedance spectroscopy data simulation in the present study was composed of resistors R and constant phase elements, CPE (symbol Q in Fig. 6). In solid materials, a distribution of relaxation times is usually observed and the capacitance is replaced by a CPE, which represents the behavior of the grain interior, grain boundary and electrode processes more accurately [25]. The CPE causes depression of the ideal semicircle, observed on the complex plane plots by an angle β. Results of the data simulation in a form of estimated parameters of the relaxation processes are given in Tab. 2, whereas the combination of the measured data and its CNLS-fit in a complex Z''–Z' plane are given in Fig. 7 (T=200°C (a), T=400°C (b), T=500°C (c)). Calculations of were performed on the base of the equivalent circuit parameters fitting and equations given elsewhere [21, 22].

The quality of the parameter fit of an equivalent circuit to a set of impedance data can be best seen in fit quality plot (FQ-plot) [14, 21, 22]. The FQ – plot shows frequency distributions of the residuals defined by:

$$\Delta_{Re,i} = \frac{Z_i^{'} - Z^{'}(\nu_i, a_k)}{|Z^{*}(\nu_i, a_k)|}, \tag{4}$$

$$\Delta_{Im,i} = \frac{Z_i^{''} - Z^{''}(\nu_i, a_k)}{|Z^{*}(\nu_i, a_k)|}, \tag{5}$$

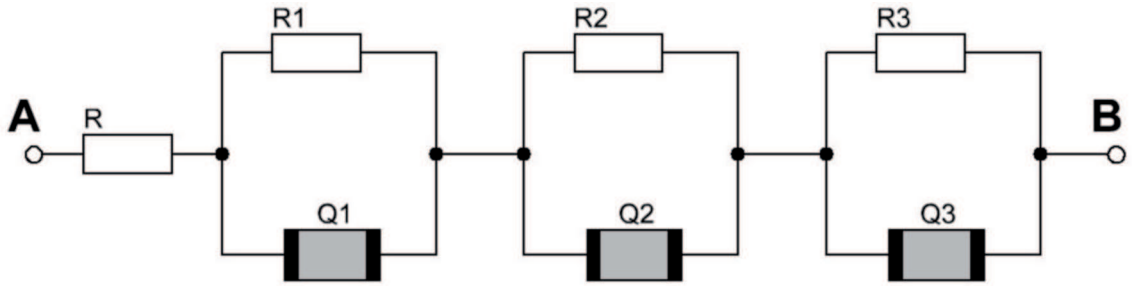

Fig. 6. Schematic representation of the equivalent circuit used in the dispersion analysis of $Bi_4Ti_3O_{12}$ ceramics within the temperature range ΔT=200–500^{0}C

TABLE 2

Estimated values of resistance (R_i), capacitance (C_i), relaxation frequency ($\nu_{max,i}$) and depression angle (β_i) calculated from equivalent electric circuit parameters. The validity of the fitting procedure was estimated by χ^2 and WSS

Parameter	T=200°C	T=400°C	T=500°C	T=550°C
R [Ω]	14.9	136.9	175.8	176.6
R_1 [Ω]	1516.3	569.1	188.6	88.4
C_1 [F]	1.75×10^{-10}	2.88×10^{-10}	6.49×10^{-10}	1.56×10^{-10}
ν_{1max} [Hz]	0.599194×10^{6}	0.970258×10^{6}	1.29957×10^{6}	1.15456×10^{6}
β_1 [deg]	23.56	14.79	3.31	-7.16
R_2 [Ω]	1867.7	682.7	270.7	177.8
C_2 [F]	1.29×10^{-8}	1.17×10^{-8}	0.88×10^{-8}	0.78×10^{-8}
ν_{2max} [Hz]	6600	19881	66866	115379
β_2 [deg]	20.23	25.89	27.53	26.11
R_3 [Ω]	3539.9	990.8	330.6	192.3
C_3 [F]	7.16×10^{-7}	6.20×10^{-7}	6.10×10^{-7}	6.80×10^{-7}
ν_{3max} [Hz]	62	259	789	1217
β_3 [deg]	35.52	37.30	49.03	52.67
WSS	1.82×10^{-4}	5.46×10^{-4}	1.55×10^{-4}	3.59×10^{-9}
χ^2	1.20×10^{-6}	3.59×10^{-6}	1.05×10^{-6}	2.42×10^{-11}

where Z', Z'' – real and imaginary components of the measured impedance, $Z^*(\nu, a_k)$ – impedance model function, a_k – parameter of the model function.

The residual are plotted against frequency (ν) on a log scale (Fig. 8). For a good fit these deviations should be distributed randomly around the frequency axis. In our experiment a clear sinusoidal type trace is seen in Fig.8 (T=200°C (a), T=400°C (b), T=500°C) (c), however, the residuals are less than 0.5%. In this connection it is worth noting that a good quality of the simulation was reached during present studies.

From the estimated values of grain, grain boundary and material/electrode interface resistances calculated from the semicircular arcs in the impedance spectrum by CNLS fitting of experimental impedance spectra to the equivalent electric circuit parameters (Tab. 2) the corresponding values of conductivity (σ) at different temperatures in the measuring range were calculated according to the general equation:

$$\sigma = \frac{l}{S \times R}, \tag{6}$$

where: l, S – dimensions, R – resistance.

(a)

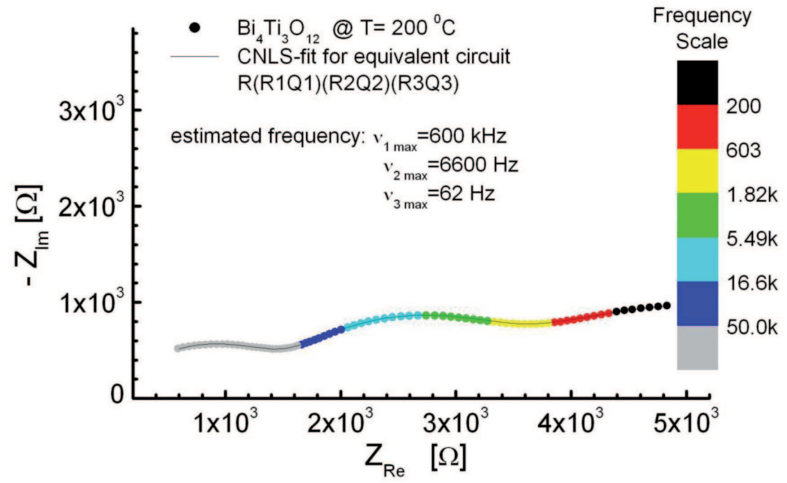

(b)

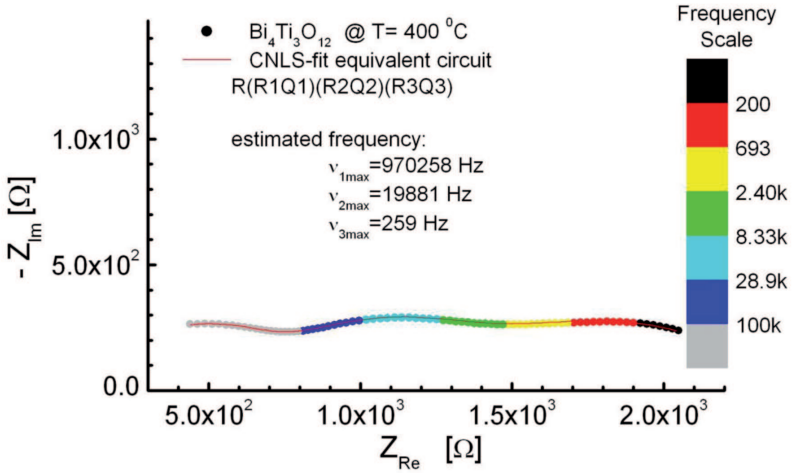

(c)

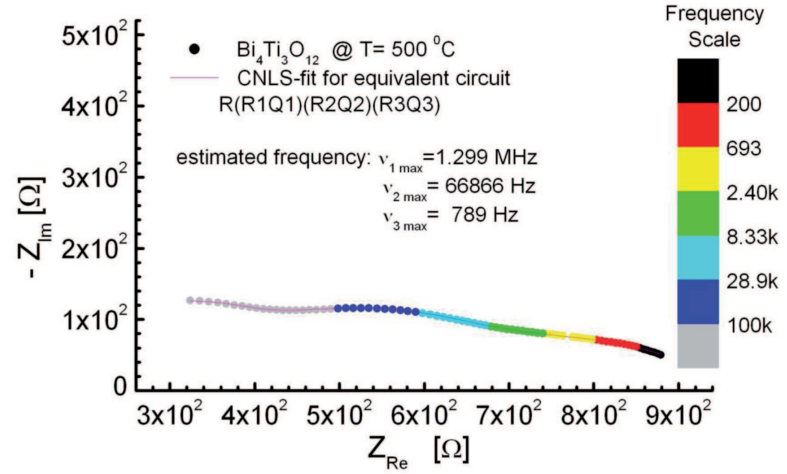

Fig. 7. Plot of Z'' vs. Z' for $Bi_4Ti_3O_{12}$ at T=200°C (a), T=400°C (b), T=500°C (c). Combination of the measured data (circles) and its CNLS-fit (line) is given

(a)

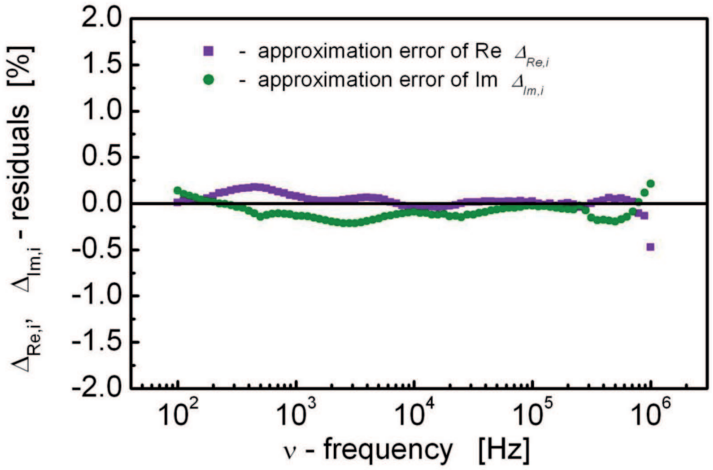

(b)

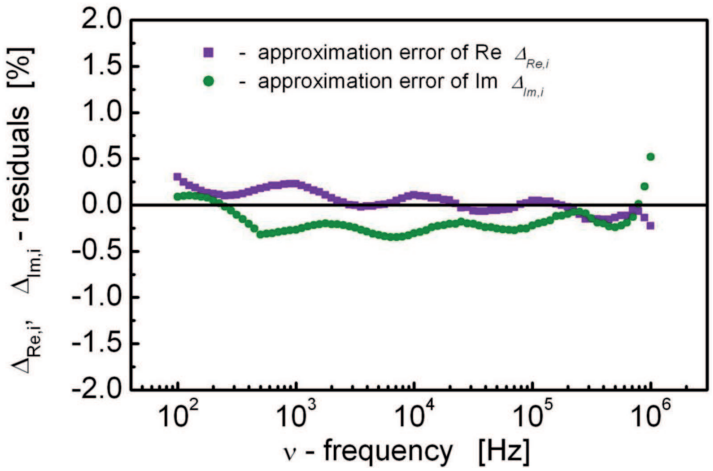

(c)

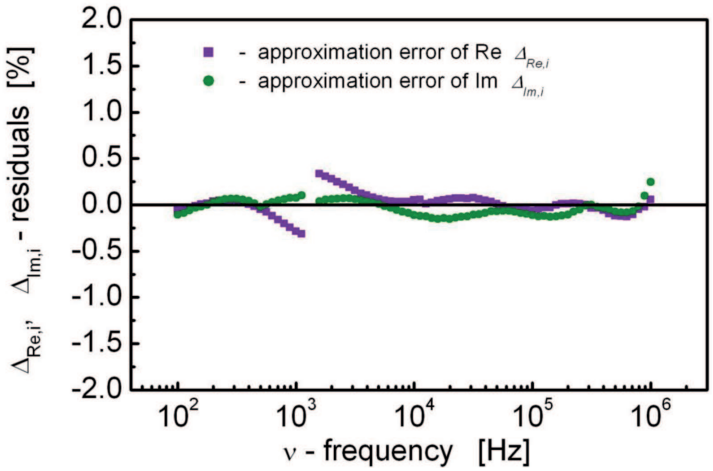

Fig. 8. FQ-plots for the final parameter set obtained with the dispersion analysis program for $Bi_4Ti_3O_{12}$ ceramics at temperature range ΔT=200–500°C (T=200°C (a), T=400°C (b), T=500°C (c))

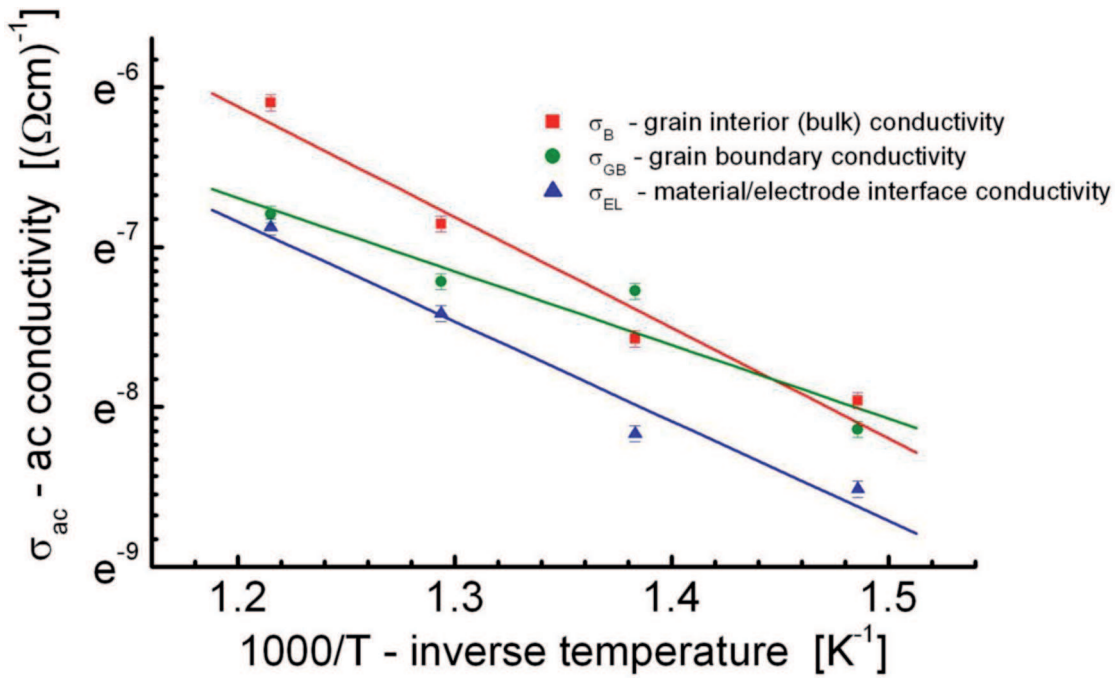

Fig. 9. Arrhenius plot of bulk (σ_B) grain boundary (σ_{GB}) and material/electrode interface (σ_{EL}) conductivity for $Bi_4Ti_3O_{12}$ ceramics

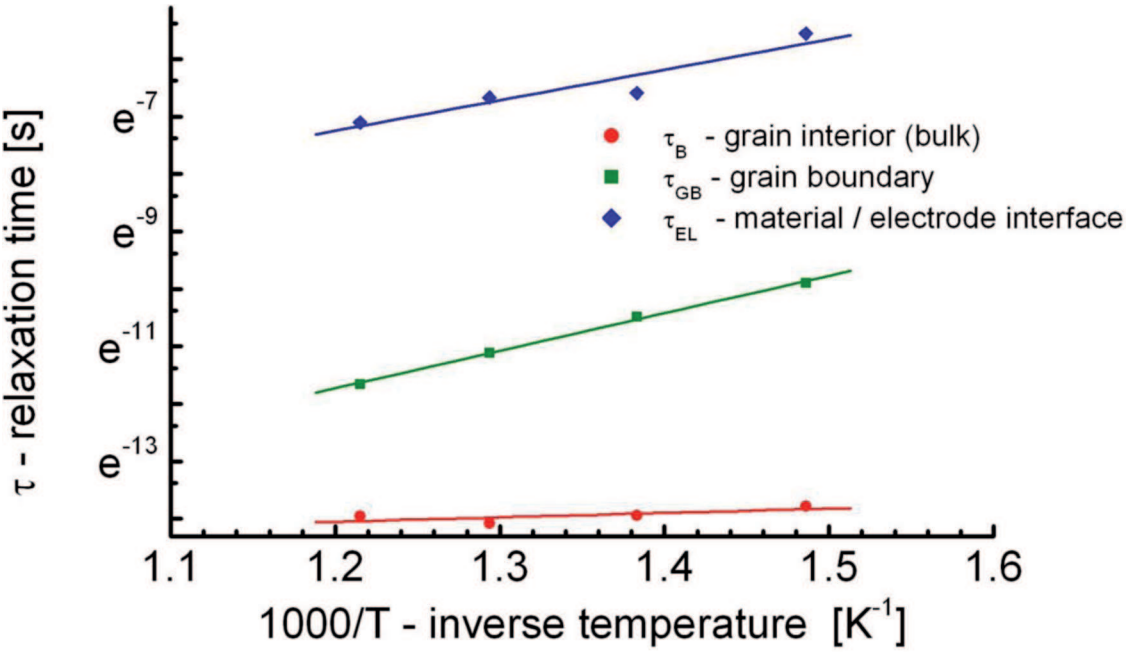

Fig. 10. Arrhenius plot of bulk (τ_B) grain boundary (τ_{GB}) and material/electrode interface (τ_{EL}) relaxation times for $Bi_4Ti_3O_{12}$ ceramics

The variation of grain (σ_B) grain boundary (σ_{GB}) and material/electrode interface (σ_{EL}) conductivity was expressed as a function of inverse absolute temperature (1000/T) and is shown in Fig. 9. The Arrhenius plot of these data made it possible to calculate the activation energy for the electrical conduction process according to the formula:

$$\sigma = \left(\frac{A}{T}\right)\exp\left(\frac{-E_a^c}{kT}\right), \tag{7}$$

where A is a constant, T the absolute temperature, E_a^c the activation energy of conductivity, and k is the Boltzmann's constant [26].

From the relaxation times, the activation energies for relaxations were calculated using the relation:

$$\tau = \tau_0 \exp\left(\frac{-E_a^t}{kT}\right), \tag{8}$$

where E_a^t is the activation energy for relaxation. Fig. 10 shows the temperature dependence of relaxation time in a log – $1/T$ scale.

The results of calculation of activation energies for both ac conductivity and relaxations for grain (bulk), grain boundary and electrode processes in polycrystalline $Bi_4Ti_3O_{12}$ ceramics are given in Tab. 3.

TABLE 3
Activation energy for bulk (E_B), grain boundary (E_{GB}) and electrode processes (E_{EL}) for $Bi_4Ti_3O_{12}$ ceramic

Parameter	E_B [eV]	E_{GB} [eV]	E_{EL} [eV]
activation energy for conductivity (σ) E_a^c	0.60	0.40	0.54
activation energy for relaxation (τ) E_a^t	0.07	0.56	0.46

E_a^c obtained in these samples in the temperature range ΔT=200-500°C is around E_a^c=0.6eV for grain interiors, E_a^c=0.4eV for grain boundaries and E_a^c=0.54eV for ceramic sample/electrode interface.

The activation energy for relaxation is about E_a^t=0.07eV, E_a^t=0.56eV and E_a^t=0.46eV for bulk, grain boundaries and electrode processes, respectively.

It is worth noting that E_a^c values of conductivity observed in the present studies are consistent with the activation energies of bismuth layer-structured ferroelectrics in which conductance is determined by oxygen vacancies [26]. It was found that the activation energies for relaxation processes differ from those obtained from conductivity plots. The activation energy for relaxation ascribed to grain boundaries is higher than the activation energy for ac conductivity, whereas in case of grain interior and material/electrode interface the activation energy of conductivity is higher than the activation energies for relaxations in the temperature range selected. In case of bulk compound activation energy for relaxation is about ten times smaller than activation energy for conductivity. Usually small activation energy is ascribed to instability in the systems [27].

Taking into consideration that both relaxation and conduction processes are dependent on defect–vacancy impurity complexes and that the space charges developed in the sample may also affect the relaxation processes–higher activation may be obtained from relaxation temperature plot in case of grain boundary component.

4. Conclusions

Bismuth titanate ($Bi_4Ti_3O_{12}$) ceramics was synthesized by the mixed oxide method. It was found that BiT ceramics sintered at T=1000°C adopted the orthorhombic symmetry of *Fmmm* space group and the following elementary cell parameters: a=5.409(6)Å, b=5.449(2)Å and c=32.816(2)Å. Impedance diagrams of $Bi_4Ti_3O_{12}$ ceramics show three overlapping semicircles that were well resolved by CNLS fitting. Each of them corresponded to the a particular microstructural region of the ceramic material, i.e. grain interior (bulk), grain boundaries and material/electrode interfaces. The proposed equivalent electric circuit consisted of a series combination of three parallel combinations of the resistance (R) and the constant-phase element (Q). The experimental response was found to be in excellent agreement with the simulated one thus indicating that the proposed model gave an adequate representation of the electrical properties of the sample. From the estimated values of resistances the corresponding values of conductivity were calculated and activation energies of both ac conductivity and relaxations were calculated.

Acknowledgements

The present research has been supported by Polish Ministry of Education and Science from the funds for science in 2008-2011 as a research project N N507 446934.

REFERENCES

[1] B. Aurivillius, Mixed bismuth oxides with layer lattices. The structure type of $CaNb_2Bi_2O_9$, Arkiv for Kemi **1**, 54, 463-480 (1949).

[2] B. Aurivillius, Mixed bismuth oxides with layer lattices. Structure of $Bi_4Ti_3O_{12}$. Arkiv for Kemi **1**, 58, 499-512 (1949).

[3] B. Aurivillius, Mixed oxides with layer lattices. Structure of $BaBi_4Ti_4O_{15}$, Arkiv for Kemi **2**, 37, 519-527 (1950).

[4] A. Lisińska-Czekaj, D. Czekaj, Synthesis of $Bi_5TiNbWO_{15}$ ceramics, Archives of Metallurgy and Materials **54**, 4, 869-874 (2009).

[5] A. Lisińska-Czekaj, M. Czaja, L. Kozielski, D. Czekaj, M. Piechowiak, M. Nowakowski, K. Zawiślok, Photoluminescence of nanocrystalline bismuth titanate thin films synthesized by the sol-gel method, Materials Science Forum **514-516**, 128-132 (2006).

[6] A. Lisińska-Czekaj, E. Jartych, M. Mazurek, J. Dzik, D. Czekaj, Dielektryczne i magnetyczne właściwości ceramiki multiferroicznej $Bi_5Ti_3FeO_{15}$, Materiały Ceramiczne **63**, 126-133 (2010).

[7] R. Waser (Ed): Nanoelectronics and informatiom technology, Wiley-VCH, Weinheim, 2005.
[8] R.E. Newnham, R.W. Wolfe, J.F. Dorrian, Structural basis of the bismuth ferroelectricity in titanate family, Materials Research Bulletin **6**, 1029 (1971).
[9] A. Lisińska-Czekaj, D. Czekaj, Z. Surowiak, Synthesis and dielectric properties of $SrBi_3Ti_2NbO_{12}$ ceramics with layer perovskite structure, Key Engineering Materials **206-213**, 1429-1432 (2002).
[10] E. Jartych, M. Mazurek, A. Lisińska-Czekaj, D. Czekaj, Hyperfine interactions in some Aurivillius $Bi_{m+1}Ti_3Fe_{m-3}O_{3m+3}$ compounds, Journal of Magnetism and Magnetic Materials **322**, 51-55 (2010).
[11] Z.S. Macedo, C.R. Ferrari, A.C. Hernandes, Impedance spectroscopy of $Bi_4Ti_3O_{12}$ ceramic produced by self-propagating high-temperature synthesis technique, Journal of the European Ceramic Society **24**, 2567-2574 (2004).
[12] A. Snedden, P. Lightfoot, T. Dinges, M. Islam, Defect and dopant properties of the Aurivillius phase $Bi_4Ti_3O_{12}$, Journal of Solid State Chemistry **177**, 3660-3665 (2004).
[13] C. Paz de Araujo, J.F. Scott, G.W. Taylor (Ed): Ferroelectric thin films: synthesis and basic properties, Gordon and Breach Publishers, Amsterdam, 1996.
[14] B. Boukamp, A nonlinear least squares fit procedure for analysis of immitance data of electrochemical systems, Solid State Ionics **20**, 31-44 (1986).
[15] P. Zoltowski, Non-traditional approach to measurement models for analysis of impedance spectra, Solid State Ionics **176**, 1979-1986 (2005).
[16] M. Guillodo, J. Fouletier, L. Dessemond, P. Del Gallo, Electrical properties of dense Me-doped bismuth vanadate (Me=Cu, Co) pO_2-dependent conductivity determined by impedance spectroscopy, Journal of the European Ceramic Society **21**, 2331-2344 (2001).
[17] M.I. Morozov, L.P. Mezentseva, V.V. Gusarov, Mechanism of formation of $Bi_4Ti_3O_{12}$, Russian Journal of General Chemistry **72**, 7, 1038-1040 (2002).
[18] M. Krzhizhanovskaya, S. Filatov, V. Gusarov, P. Paufler, R. Bubnova, M. Morozov, D.C. Meyer, Aurivillius phases in $Bi_4Ti_3O_{12}/BiFeO_3$ system: thermal behaviour and crystal structure, Zeitschrift Fur Anorganische Und Allgemeine Chemie **631**, 1603-1608 (2005).
[19] N.A. Lomanova, M.I. Morozov, V.L. Ugolkov, V.V. Gusarov, Properties of Aurivillius phases in the $Bi_4Ti_3O_{12}$- $BiFeO_3$ system, Inorganic Materials **42**, 2, 189-195 (2006).
[20] H. Bernard, J. Dzik, A. Lisińska-Czekaj, K. Osińska, D. Czekaj, Zastosowanie metody MOM do wytwarzania ceramiki $Bi_4Ti_3O_{12}$, Inżynieria Materiałowa **178**, 6, 1404-1408 (2010).
[21] D. Czekaj, A. Lisińska-Czekaj, T. Orkisz, J. Orkisz, G. Smalarz, Impedance spectroscopic studies of sol-gel derived barium strontium titanate thin films, Journal of the European Ceramic Society **30**, 465-470 (2010).
[22] B. Wodecka-Duś, D. Czekaj, Fabrication and dielectric properties of donor doped $BaTiO_3$ ceramics, Archives of Metallurgy and Materials **54**, 923-933 (2009).
[23] B.A. Boukamp, Electrochemical impedance spectroscopy in solid state ionics; Recent advances, Solid State Ionics **169**, 1-4, 65-73 (2004).
[24] B.A. Boukamp, A linear Kronig–Kramers transformation test for immitance data validation, Journal of the Electrochemical Society **142**, 6, 1885-1894 (1995).
[25] A. Lasia, Electrochemical impedance spectroscopy and its applications. In: Modern Aspects of Electrochemistry (ED): B.E.Conway, J.O.M.Bockris and R.E.White, Kluger Academic/Plenum Publishers, New York 1999.
[26] E. Venkata Ramana, S.V. Suryanarayana, T. Bhima Sankaram, AC impedance studies on ferroelectromagnetic $SrBi_{5-x}La_xTi_4FeO_{18}$ ceramics, Materials Research Bulletin **41**, 1077-1088 (2006).
[27] R. Machado, M.G. Stachiotti, R.L. Migoni, A. Huanosta Tera, First principles determination of ferroelectric instabilities in Aurivillius compounds, Physical Review **B70**, 214112-1-214118-8 (2004).

Received: 20 March 2011.